AIP | Applied Physics Letters

Size effect of flexible proof mass on the mechanical behavior of micron-scale cantilevers for energy harvesting applications

Miso Kim, Seungbum Hong, Dean J. Miller, John Dugundji, and Brian L. Wardle

Citation: Appl. Phys. Lett. **99**, 243506 (2011); doi: 10.1063/1.3663858
View online: http://dx.doi.org/10.1063/1.3663858
View Table of Contents: http://apl.aip.org/resource/1/APPLAB/v99/i24
Published by the American Institute of Physics.

Size effect of flexible proof mass on the mechanical behavior of micron-scale cantilevers for energy harvesting applications

Miso Kim,[1,2,a)] Seungbum Hong,[2] Dean J. Miller,[2] John Dugundji,[3] and Brian L. Wardle[3]
[1]*Department of Materials Science and Engineering, MIT, Cambridge, Massachusetts 02139, USA*
[2]*Materials Science Division, Argonne National Laboratory, Lemont, Illinois 60439, USA*
[3]*Department of Aeronautics and Astronautics, MIT, Cambridge, Massachusetts 02139, USA*

(Received 22 June 2011; accepted 26 October 2011; published online 15 December 2011)

Mechanical behavior of micron-scale cantilevers with a distributed, flexible proof mass is investigated to understand proof mass size effects on the performance of microelectromechanical system energy harvesters. Single-crystal silicon beams with proof masses of various lengths were fabricated using focused ion beam milling and tested using atomic force microscopy. Comparison of three different modeling results with measured data reveals that a "two-beam" method has the most accurate predictive capability in terms of both resonant frequency and strain. Accurate strain prediction is essential because energy harvested scales with strain squared and maximum strain will be a design limit in fatigue. © *2011 American Institute of Physics*. [doi:10.1063/1.3663858]

As the microelectromechanical system (MEMS) device dimensions scale down, the natural frequencies of these devices can approach the GHz range.[1] A beam end mass, i.e., a proof mass, is integral to tune device resonances towards target frequency points for practical applications such as energy harvesters where oftentimes output power density (power spectral density) falls off as frequency increases.[2] The role of proof mass becomes significant particularly in realizing MEMS piezoelectric vibration energy harvesters (PVEHs) since it enables not only harvesting of low-level vibrations by serving to decrease the resonant frequency but also generation of increased power by raising the average level of inner stress and strain along the beam length. While it is common to integrate a proof mass at the end of the MEMS-scale cantilevers to obtain the target frequency of interest,[3,4] insufficient attention has been paid to a rigorous analytical treatment of a proof mass.

The most common approach to calculate the resonant frequency of a cantilever with a proof mass is to simply approximate a concentrated proof mass at a subjectively chosen point on the beam and to consider the effective mass of the system.[5,6] Such a concentrated mass model is not capable of capturing the structural dynamics that result from geometric properties of a distributed proof mass. In a more sophisticated approach,[7] a rigid proof mass with rotational terms is considered, which eliminates the necessity of choosing an arbitrary point for a center-of-mass calculation. This provides a more accurate prediction for both resonant frequencies and device performance. It was shown that even a small change in proof mass geometry results in a substantial change in device performance due to both the frequency shift and the effect on the strain distribution along the device length, suggesting the importance of appropriate treatment of the proof mass configuration in device design.

In this work, we develop a more rigorous model that considers a flexible proof mass for a micron-scale cantilever where the proof mass also contributes to the bending stiffness of the system. Long, thin, distributed proof masses are quite common in MEMS devices due to the constraints of thin-film processing.[3,4] A cantilevered device with a proof mass is modeled as two joined beams with different uniform cross-sections (Fig. 1). L_0 and L_{PM} represent the length of the beam without a proof mass (beam 1) and the length of a proof mass (beam 2), whereas L is the total length of the entire device. The axial beam coordinate is denoted as x while z indicates the transverse coordinate along which direction bending of a cantilever occurs. A sinusoidal base-excitation induces mechanical vibration of the beam, where $\ddot{w}_B$ represents base acceleration. Beam displacement, w, can be defined as displacement relative to the base of the cantilever.

For the vibration analysis, the Nth mode of the mechanical mode shapes of each beam is expressed as $\psi_{N,1}$ for beam 1 and $\psi_{N,2}$ for beam 2 with a set of constants representing modal amplitudes, c, d, e, f and $\bar{c}$, $\bar{d}$, $\bar{e}$, $\bar{f}$, respectively, as shown in Eqs. (1) and (2)

$$\psi_{N,1} = c\sinh\lambda_{N,1}x + d\cosh\lambda_{N,1}x + e\sin\lambda_{N,1}x + f\cos\lambda_{N,1}x, \tag{1}$$

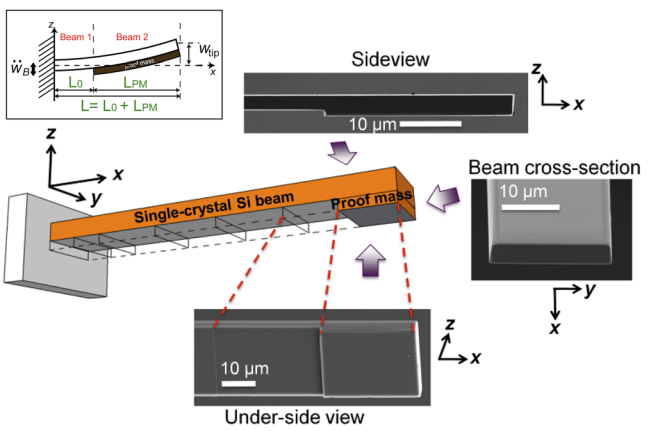

FIG. 1. (Color online) 3-D schematic and SEM images of a single-crystal silicon cantilever with a flexible, distributed, thin proof mass fabricated by FIB lithography. Inset shows 2-D schematic of base-excited cantilevered beam with a proof mass at the tip with defined parameters.

a)Author to whom correspondence should be addressed. Electronic mail: misokim@mit.edu.

$$\psi_{N,2} = \bar{c}\sinh\lambda_{N,2}x + \bar{d}\cosh\lambda_{N,2}x + \bar{e}\sin\lambda_{N,2}x + \bar{f}\cos\lambda_{N,2}x. \quad (2)$$

Euler-Bernoulli beam theory enables determination of the mechanical mode shape following the relations in Eqs. (3) and (4). $\overline{EI}$ is the effective bending stiffness, which is obtained considering the neutral axis and the properties of the beam (or plate) multi-layers, while m is mass per length for each beam (or plate).[8] ω_N [rad/s] represents the Nth mode resonance frequencies.

$$(\overline{EI})_1\psi^{IV}_{N,1} - m_1\omega_N^2\psi_{N,1} = 0 \quad 0 \le x \le L_0, \quad (3)$$

$$(\overline{EI})_2\psi^{IV}_{N,2} - m_2\omega_N^2\psi_{N,2} = 0 \quad L_0 \le x \le L. \quad (4)$$

Boundary conditions at the fixed end, free end, and the junction between beam 1 and beam 2 are established, considering the clamping (Eq. (5)), bending moment and shear force at the tip (Eq. (6)), and continuity condition for displacement, slope, bending moment, and shear force at the junction, $x = L_0$ (Eq. (7))

$$\text{At } x = 0,\ \psi_{N,1} = 0 \text{ and } \psi'_{N,1} = 0. \quad (5)$$

$$\text{At } x = L,\ (\overline{EI})_2\psi''_{N,2} = 0 \text{ and } (\overline{EI})_2\psi'''_{N,2} = 0. \quad (6)$$

$$\text{At } x = L_0,\ \psi_{N,1} = \psi_{N,2},\ \psi'_{N,1} = \psi'_{N,2},\ (\overline{EI})_1\psi''_{N,1} = (\overline{EI})_2\psi''_{N,2},\ \text{and } (\overline{EI})_1\psi'''_{N,1} = (\overline{EI})_2\psi'''_{N,2} \quad (7)$$

where $()' = \partial/\partial x$. These boundary conditions give eight equations which can be reduced to an 8×8 matrix. The determinant of this matrix gives successive values of a parameter $\bar{\lambda}_N$, which can be related to the original parameter $\lambda_{N,1}$ and $\lambda_{N,2}$. Once the parameter, $\bar{\lambda}_N$, is known, both mode shape and the resonance frequency for the Nth mode are readily obtainable. The first resonance frequency, f_1, for example, is given by Eq. (8)

$$f_1 = \frac{1}{2\pi}\omega_1 = \frac{1}{2\pi}(\bar{\lambda}_1)^2\sqrt{\frac{(\overline{EI})_1}{m_1L^4}} \text{ [Hz]} \quad (8)$$

For practical use, we normalize the mode shape to $\psi_N(L) = 2$ at the tip as is common practice in beam dynamics.[8,9] Based on this modal analysis, we can predict mechanical performance of a cantilever such as resonant frequencies, mechanical mode shape, and strain distribution along the beam depending on various sizes of flexible proof masses. While dynamic stiffness method developed by Bonello and Rafique previously enables analysis of cantilevered system with two different cross-sections, they did not explicitly solve the problem of size effects of flexible proof masses.[10] The flexible proof mass analysis based on the two-beam method not only has the capability to characterize the structural dynamics of cantilevered systems with two different cross-sections but also can be extended to 3-beam systems that consist of cantilever with piezoelectric patches as well as proof masses.

In order to verify this model for a flexible proof mass as well as to investigate the mechanical behavior of micron-scale cantilevers with a distributed, flexible proof mass, tip-less single-crystal silicon cantilever probes (Nanosensor, TL-FM 20) for atomic force microscopy (AFM) were modified to have proof masses of various lengths using focused ion beam milling (FIB, Zeiss NVision 40). Edge-on milling for accurate dimension control was carried out at 30 kV with a probe current of 13 nA for initial trimming of tip-less cantilevers and 700 pA for sequential subtraction (see Fig. 1). Scanning electron microscope (SEM) images were collected at each stage to provide dimensions of the system. The micro-machined cantilever probes with proof masses of different lengths were mounted in AFM (MFP-3D, Asylum Research) to measure their resonant frequencies.

In Fig. 1, we illustrate a cantilever with a relatively thin, distributed proof mass of different lengths with SEM images of one proof mass case ($L_{PM} = 28.5\ \mu$m) from different perspectives. Starting from a uniform beam where total length of the beam is 220.7 μm and the total thickness is 3.07 μm, we milled out sequentially in length from the clamped end, thus resulting in a set of cantilevers with proof mass lengths of 200, 181.3, 140.3, 99.7, 59.2, 28.5 μm, and lastly a cantilever with no proof mass (1.94 μm in average thickness). The width of the cantilever was measured to be 20.7 μm on average. There are two aspects noteworthy in SEM images of Fig. 1. First of all, a small step-like trace remained visible for each segment that was milled away as it is hard to control the milling thickness and orientation of the sample perfectly to match with the previous segment. Therefore, when we implement our model to calculate resonant frequency, the average beam thickness of 1.13 μm was used as the thickness of a proof mass, thus giving a total thickness, 3.07 μm for the beam plus proof masses. Second, it is quite notable that no bending was observed even after all milling process, implying that little residual stress is induced even when significant amount of single-crystal Si beam is etched by Ga ions.

First-mode resonant frequencies were measured and compared with simulated results from three different modeling approaches on the cantilevers with proof masses of various lengths. These results are shown in Fig. 2 where resonant frequencies are plotted against normalized length of proof mass (i.e., ratios of length of proof masses (L_{PM}) to the total length of the system (L)). Density and elastic modulus

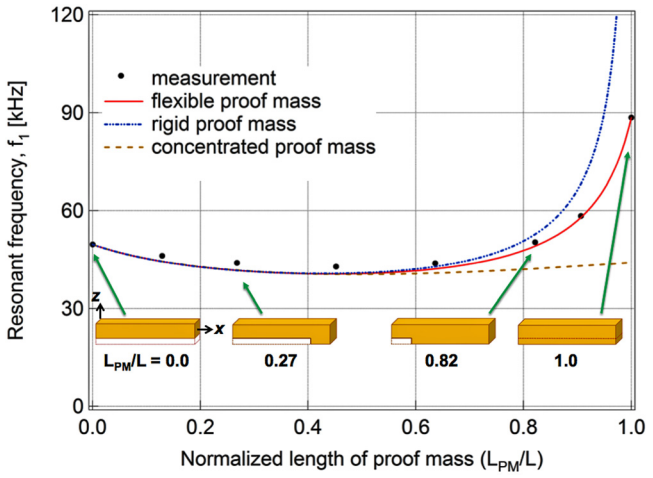

FIG. 2. (Color online) Resonant frequency, f_1 vs. normalized length of proof mass, L_{PM}/L: simulated vs. experiments.

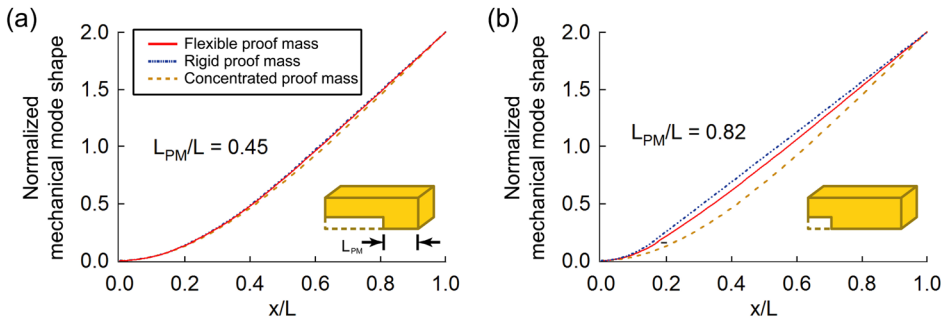

FIG. 3. (Color online) Normalized mechanical mode shape along the normalized beam length (x/L) at various sizes of proof mass.

are required as modeling inputs. 2329 kg/m^3 is used as the density of single-crystal Si.[9] Elastic modulus of single-crystal silicon in [001] direction is estimated by using the 1st resonant frequency that is experimentally obtained at both end points.[9,10] 88.6 kHz is obtained at the right ending point ($L_{PM} = 220.7\ \mu$m) while 49.6 kHz is recorded at the left ending point ($L_{PM} = 0.0\ \mu$m), each providing 176.0 GPa and 138.4 GPa, respectively, which are in the range of the reported values for single-crystal Si of this orientation, 125 GPa-179 GPa.[11] The reason for the change in elastic properties between these ending points can be explained by the effect of Ga ions during FIB lithography.[12] Therefore, we take 138.4 GPa for the elastic modulus of beam (beam 1) where Ga ions cause the material property to change while we use 176.0 GPa for the second beam (proof mass region) which is unaffected by FIB milling. In Fig. 2, comparison of three different modeling results with the experimentally measured values suggests that each model has good predictive capability of resonant frequencies up to the point when the size of proof mass occupies ~60% of the total cantilever, despite the significant approximations in those models. However, a discrepancy between the modeling results and the measured values becomes prominent once the proof mass gets longer and more distributed than 60% of the total length. For instance, the resonant frequency predicted by the flexible proof mass analysis is in much better agreement with the measured frequency (1% of difference vs. 26% by concentrated proof mass analysis and 17% by rigid proof mass analysis when normalized proof mass length is 0.82). From the perspective of predicting dynamics (e.g., estimation of resonant frequencies), Fig. 2 would seem to indicate that a refined "two-beam" dynamic model is of little value except when very long and thin proof masses are considered.[13] However, prominent differences occur when it comes to prediction of strains (and therefore energy harvested in the case of, e.g., a PVEH) depending on the choice of model.

In Fig. 3, mechanical mode shapes obtained from three different proof mass analyses are shown against x/L, the axial position of normalized length of the entire cantilever, where 0.0 and 1.0 indicate the fixed end and the very end of the beam (or end of the proof mass), respectively, for various lengths of proof masses. Mechanical mode shape, ψ_r, plays a major role in describing not only the structural dynamics of general cantilever system but also the device performance PVEHs.[8] The longer a proof mass becomes, the greater the difference in mechanical mode shapes predicted by the different modeling approaches. As shown in Fig. 4, the difference among modeling methods becomes even more distinct in the prediction of beam curvature (2nd derivative of mechanical mode shapes), which is directly related to axial strain when the length of proof mass increases.[8] Accurate estimate of strain is significant because it helps control fatigue and, therefore, design against structural failure during vibrating operation. Moreover, more power can be extracted in PVEHs at larger strains as it scales with strain squared.[8] Comparison of the absolute magnitudes of strain in Fig. 4 suggests that the longer and distributed proof mass induces more strain, implying increased power generation of piezoelectric energy harvesters. In Fig. 4, the flexible proof mass analysis accounts for the strain distribution in detail over the entire cantilever including the proof mass region where discontinuities along x indicates the juncture of the proof mass and active beam. In contrast, neither the concentrated nor the rigid proof mass analysis includes the strain distribution under the proof mass area. It is also seen in Fig. 4 that when normalized proof mass length is 0.82, predicted maximum strain at the fixed end of a cantilever can differ up to 40% depending on analytical approach for proof mass, underscoring the importance of appropriate treatment of flexible proof mass in MEMS-scale systems.

Future work will include the model-experiment comparison study of the proof mass effects of a cantilevered system

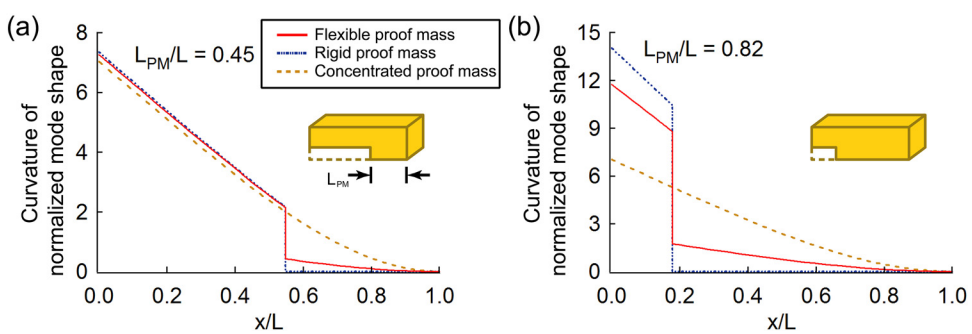

FIG. 4. (Color online) Curvature of normalized mode shape along the normalized beam length (x/L) at various sizes of proof mass.

on the behavior of tip displacement[14] and structural mode shapes, based on the two-beam method modeling.

AFM and FIB experiments were carried out in Materials Science Division and Electron Microscopy Center at Argonne National Laboratory, a U.S. DOE Office of Science Laboratory, operated under Contract No. DE-AC02-06CH11357.

[1]H. G. Craighead, Science **290**, 1532 (2000).
[2]N. E. du Toit, B. L. Wardle, and S.-G. Kim, Integr. Ferroelectr. **71**, 121 (2005).
[3]D. Shen, J.-H. Park, J. Ajitsaria, S.-Y. Choe, C. W. III Howard, and D.-J. Kim, J. Micromech. Microeng. **18**, 055017 (2008).
[4]L.-P. Wang, K. Deng, L. Zou, R. Wolf, R. J. Davis, and S. Trolier-McKinstry, IEEE Electron Device Lett. **23**, 182 (2002).
[5]J. E. Sader, I. Larson, P. Mulvaney, and L. R. White, Rev. Sci. Instrum. **66**, 3789 (1995).
[6]J. W. Yi, W. Y. Shih, and W.-H. Shih, J. Appl. Phys. **91**, 1680 (2002).
[7]M. Kim, M. Hoegen, J. Dugundji, and B. L. Wardle, Smart Mater. Struct. **19**, 045023 (2010).
[8]D. J. Inman, *Engineering Vibration* (Prentice Hall, Upper Saddle River, 1996).
[9]L. Meirovitch, *Fundamentals of Vibrations* (McGraw-Hill, New York, 2000).
[10]P. Bonello and S. Rafique, ASME J. Vib. Acoust. **122**, 011009 (2011).
[11]B. Bhushan and X. Li, J. Mater. Res. **12**, 1 (1997).
[12]H. Bei, S. Shim, M. K. Miller, G. M. Pharr, and E. P. George, Appl. Phys. Lett. **91**, 111915 (2007).
[13]S. Roundy, P. K. Wright, and J. M. Rabaey, *Energy Scavenging for Wireless Sensor Networks* (Kluwer Academic, Boston, 2004).
[14]Y. Chen, A. J. Dick, and F. H. Ghorbel, Smart Mater. Struct. **18**, 115012 (2009).